A Dynamic Model of a High Temperature Arc Lamp

B. Halliop, F. P. Dawson, IEEE Senior Member, and M. C. Pugh

Abstract— High temperature, high pressure arc lamps are used to thermally process semiconductor wafers. An accurate dynamic model that links radiation output to current input would facilitate the design of a power circuit that optimizes energy transfer to the arc. A finite volume arc model was derived using averaging of the energy balance equation over spatial domains. The space averaging approach accurately models the partial differential equation form of the energy balance equation, as tested with both steady state and transient arc currents, including high energy pulses with a current amplitude range from 400A to 40kA and a pulse width of a millisecond or less

Index Terms—arc lamp, finite volume method

I. INTRODUCTION

A high temperature, high pressure arc lamp is used for rapid thermal processing of semiconductor wafers. The lamp uses rapid pulses of optical radiation to heat the surface of the wafer to a high temperature in a short period of time, thus limiting diffusion of materials into the wafer. The current through the arc is pulsed from a simmer current of approximately 400A to as much as 40kA and back in a time on the order of 1 ms [1]. Power circuits that can control the flow of energy to the arc are required to power the lamp, so that the desired wafer temperature distribution can be obtained. An accurate dynamic model of the argon arc that links radiation output to current input would aid in the design of such power circuits.

Existing arc models used in power circuit designs are empirical. The coupling between the electric and heat flux density fields is not included. Therefore the temporal evolution of the optical output cannot be determined.

Existing design procedures for designing pulse-forming networks for flash lamps are well known. These methods are based on a quasi steady state model of the arc. For example, for a single mesh L/C drive circuit, J.P. Markiewicz and J.L. Emmet have defined formulas to describe the lamp electrical behavior and to choose appropriate L and C values, in Equations (1) to (5) [2].

Arc voltage is assumed to be given by:

$$v = \pm K_o (i)^{0.5} \tag{1}$$

This equation is used to describe the arc if the current density is greater than 500A/cm^2. K_o is known as the impedance parameter and is defined in (2).

$$K_o = 1.28(\frac{P}{K_1})^{0.2} \frac{l_{arc}}{d} \tag{2}$$

P is fill pressure (torr), l_{arc} is arc length (mm), d is bore diameter (mm), and K_1 is a constant which is different for each gas.

Given the arc characterization in (1) and (2), the capacitor value for a simple LC pulser can then be chosen as follows:

$$C_{ch} = \frac{[2U_{ch} a^4 \tau^2]^{0.33}}{K_o^4} \tag{3}$$

U_{ch} is the stored energy (joules), a is a damping parameter which is 0.8 for critical damping, and τ is a time parameter in seconds, corresponding to 1/3 of the desired pulse width. If the pulse is approximately sinusoidal then the pulse width can be described as half a period of a sinusoidal wave. Thus τ is 1/6 of the period or approximately $1/2\pi$ times the period, leading to (4).

$$L_{ch} = \frac{\tau^2}{C_{ch}} \tag{4}$$

The initial voltage V_{ch} across the storage capacitor can be calculated as follows:

$$V_{ch} = (\frac{2U_{ch}}{C})^{0.5} \tag{5}$$

According to [2], Equations (1) to (5) give good first order approximations and can be used to predict the shapes of current pulses, although they do not incorporate arc dynamics. This type of modeling approach cannot be used to optimize the pulse forming network for optimum energy transfer from the electrical supply to the wafer via infrared radiation.

A number of mathematical models exist to describe dynamic arc behavior. The most commonly used arc models are the Cassie, Mayr, and Cassie-Mayr models. Other existing dynamic models are primarily modifications or combinations of these models.

Manuscript received Jun 2008.

B. Halliop is a PhD student with the Department of Electrical and Computer Engineering, University of Toronto (e-mail: basia.halliop@utoronto.ca).

F.P. Dawson is with the Department of Electrical and Computer Engineering, University of Toronto (e-mail: dawson@ele.utoronto.ca).

M.C. Pugh is with the Department of Mathematics, University of Toronto (e-mail: mpugh@math.utoronto.ca).

A. Cassie Model

Cassie investigated high current arcs [3], [4] and assumed that their power losses were mainly a result of convection losses. The arc is assumed to maintain a relatively constant temperature and conductivity, and as the current i increases, the arc diameter increases, leading to an increase in conductance G_c.

An arc time constant, θ, is given by the ratio of energy stored, U_{arc}, to power loss, Q_{loss} (6).

$$\theta = \frac{U_{arc}}{Q_{loss}} \tag{6}$$

The steady-state electric field E_{ss}, remains relatively constant, and v is the arc voltage. The Cassie model is represented by the following equation:

$$\frac{1}{G_c}\frac{d}{dt}G_c = \frac{1}{\theta}\left(\frac{iv}{G_c E_{ss}^2} - 1\right) \tag{7}$$

B. Mayr Model

Mayr [3], [4] investigated small current arcs and assumed that thermal conduction was the primary form of power loss. In this case, the cross-sectional area of the arc does not have a strong impact on the arc conductance, and can be assumed to be constant. In Mayr's arc model, electrical conductivity is dependent on temperature, and temperature varies in both time and space. Mayr modeled power loss, Q_{loss}, as constant. The Mayr model is described by the following equation:

$$\frac{1}{G_m}\frac{d}{dt}G_m = \frac{1}{\theta}\left(\frac{iv}{Q_{loss}} - 1\right) \tag{8}$$

C. Cassie-Mayr Model

The Cassie model is valid primarily at high currents and the Mayr model at small currents, near the current zero [3, 4]. To cover a larger range of arc behavior, the Cassie and Mayr models may be combined. G_m, the Mayr conductance, is used for the small-current region, and G_c, the Cassie conductance, is used for the high-current region. This may be accomplished in different ways. In the case where G_c and G_m can be isolated or approximated, they can be combined in series as in (9). The contribution to G_{cm1} (the conductance of the series Cassie-Mayr model) will be dominated by G_c in the high current region and by G_m in the small current region, with a smooth transition in between [3, 4].

$$\frac{1}{G_{cm1}} = \frac{1}{G_c} + \frac{1}{G_m} \tag{9}$$

Another model [4] that demonstrates the combined Cassie and Mayr behavior is defined in Equation (10). The time constant and power loss are both assumed to vary with the conductance, according to experimentally defined constants α and β. The time constant for this model is now a function $\theta = \theta_0 (G_{cm2})^{\beta}$ and the power loss is $Q_{loss} = N_0 (G_{cm2})^{\alpha}$.

$$\frac{1}{G_{cm2}}\frac{dG_{cm2}}{dt} = \frac{1}{\theta_0 (G_{cm2})^{\beta}}\left(\frac{iv}{N_0 (G_{cm2})^{\alpha}} - 1\right) \tag{10}$$

Models derived from physical principles can give more accuracy for a greater range of situations, can be used to better predict wafer heating and can be represented in a circuit or state space form and imported as a macro into a circuit simulator. This paper presents a dynamic model of a high pressure arc lamp that is derived from first principles and can be designed to meet a specific accuracy requirement. A finite volume arc model was derived using averaging of the energy balance equation over spatial domains.

The specific contribution of this paper is to define the method for deriving a space averaged arc model. The method used is one which employs physical and geometric data to set the coefficients in the equations thus avoiding the problem of system identification. This model is in a form that can be expressed with a circuit, while giving the expected v versus i and optical output characteristics.

II. Description of Model

The lamp is cylindrical in shape with current flow in the axial direction, as shown in Figure 1. The lamp consists of a hollow quartz cylinder where argon gas is pumped in near the cathode and out near the anode. In this particular lamp, water is used for cooling and to protect the quartz tube; a stream of water is swirled around the inside surface of the quartz tube, creating a sheet of water between the argon arc and the quartz tube. In the model described in this paper, the water is assumed to hold the outer edge of the arc at a constant temperature. In reality, the water wall will be partially vaporized and so the lamp will be a mixture of argon and water vapor, however in this paper water-wall mixing is not considered. End effects are initially neglected, as is the movement of gas along pressure gradients in the radial, circumferential and axial directions. The end effects can be treated separately and then the voltage drop across these regions can be added to the arc voltage. These assumptions thus imply that there is no heat or radiation flowing into or out of the arc in an axial direction and hence the arc has a temperature dependency only in the radial direction. A per unit length model of the lamp is sought. The main goal of this paper is to demonstrate that the modeling concept described is feasible: the process could be generalized to include other coupling terms in the future.

A. Energy Balance Equation

The law of conservation of energy is used as a basis for the model. T is temperature, C_p is the heat capacity, ρ is the density, κ is the thermal conductivity, σ is the electrical conductivity, and ε_0 is the net radiative emissivity. The transport and thermodynamic coefficients are all nonlinear functions of temperature. The energy balance equation for any point in the lamp is described by equation (11). The constitutive equation for the electric field is described by

equation (12); the integral is over the volume of the arc. The temperature is constant on the arc walls; an adiabatic boundary condition is applied on both ends of the arc.

$$C_p(T)\rho(T)\frac{\partial T}{\partial t}-\nabla\bullet(\kappa(T)\nabla T)=\sigma(T)E(t)^2-4\pi\varepsilon_0(T) \quad (11)$$

$$E(t)=\frac{i_{in}(t)}{\iiint\sigma(T)dxdydz}=\frac{i_{in}(t)}{G(t)} \quad (12)$$

B. Spatial Integration

Spatial integration of equations (11) and (12) is used to transform the partial differential equation into a set of ordinary differential equations. The lamp cross-section is divided into nested concentric shells (shown in Figure 2), and an integrated energy equation is found for each region. The temperature, T, is assumed independent of length and angle, resulting in equations defined per unit length.

Integrating equation (11) over a shell and applying the divergence theorem yields equation (13) for the region j between radii r_j and r_{j+1}.

$$-2\pi r\kappa\frac{\partial T}{\partial r}\Big|_{r_{j+1}}+2\pi r\kappa\frac{\partial T}{\partial r}\Big|_{r_j}=A_j(\bar{\sigma}\bar{E}^2(t)-4\pi\bar{\varepsilon}_0)-A_j\overline{(C_p\rho\frac{\partial T}{\partial t})} \quad (13)$$

Here, $A_j=\pi(r_{j+1}^2-r_j^2)$ is the cross-section area and the overline is the cross-section average.

C. Thermal Circuit Model

Given a shell of thickness Δ, if functions f and g are smooth enough then $\overline{fg}=\bar{f}\bar{g}+O(\Delta^2)$. Therefore for a thin shell, the approximation in (14) is made

$$\overline{C_p(T)\rho(T)\frac{\partial T}{\partial t}}=\overline{C_p(T)\rho(T)}\overline{\frac{\partial T}{\partial t}}=\overline{C_p(T)\rho(T)}\frac{\partial\bar{T}}{\partial t} \quad (14)$$

Equation (13) can be used to define a circuit where the equation describes the current entering node A in Figure 3. The thermal circuit for each region can be connected in series to give a thermal circuit representation of the entire lamp.

It remains to present a circuit for the electrical field given by equation (12). The conductances (15) for each region are connected in parallel to form a circuit describing the per-unit length electrical behavior of the lamp. The average is taken over each shell. See Figure 4.

$$G_j=A_j\sigma(T)_j \quad (15)$$

The electrical and thermal circuits are linked through the temperature and electric field. The thermal resistances and capacitances, the controlled current source, and the electrical conductances are all dependent on temperature. The controlled current source is dependent on temperature and electric field.

D. Ordinary Differential Equation Model

For a division of the lamp into *n* regions, the combined circuit model of the lamp describes a system of *n+1* equations: *n* differential equations for the thermal behavior and one algebraic equation for the electrical circuit. The radii determining the *n* regions are $0<\delta=r_1<r_2<\ldots<r_n<r_{n+1}=R$ where *R* is the radius of the lamp. The midpoint of each region is $r_{midj}=(r_j+r_{j+1})/2$.

The first step in approximating equation (13) on the region bounded by r_j and r_{j+1} is to approximate each mean value on the right-hand side of (13) with the corresponding functions evaluated at the midpoint r_{midj}. By the Integral Mean Value Theorem ([5], page 4), each of these mean values will be achieved at some point within the region; for a sufficiently thin shell, this point can be approximated by the midpoint of the shell: r_{midj}.

The second step is to find an approximation for the each of the conductive heat loss terms on the left-hand side of (13):

$$2\pi r\kappa(T)\frac{\partial T}{\partial r}\Big|_{r_j} \quad (16)$$

The natural finite-difference approximation would be

$$2\pi r_j\frac{\kappa(T_{mid(j-1)})+\kappa(T_{midj})}{2}\frac{T_{midj}-T_{mid(j-1)}}{r_{midj}-r_{mid(j-1)}} \quad (17)$$

However, this expression is not easily implemented in a circuit. Instead, an approach based on thermal resistance is used: the conductive heat loss is approximated by

$$Q_{condj}=\frac{T_{midj}-T_{mid(j-1)}}{R_{inj}+R_{outj}},\qquad 2\le j\le n \quad (18)$$

where R_{inj} and R_{outj} are the thermal resistances of half of the inner shell whose outer wall radius is r_j and half of the outer shell whose inner wall radius is r_j, respectively. These are found by approximating the thermal resistance ([6], §3.3) for a shell of inner radius r_a and outer radius r_b with constant conductance κ

$$R_{ab}=\frac{\ln(r_b/r_a)}{2\pi\kappa} \quad (19)$$

and then assuming that the ratio between r_b-r_a and r_a is much less than one, a Taylor expansion of equation (19) results in

$$R_{outj}=\frac{r_j-r_{j-1}}{4\pi r_j\kappa(T_{mid(j-1)})}\qquad 2\le j\le n+1 \quad (20)$$

$$R_{inj}=\frac{r_{j+1}-r_j}{4\pi r_j\kappa(T_{midj})}\qquad 1\le j\le n \quad (21)$$

n differential equations are generated, one for each region. The innermost region and outermost regions have different structures than the other regions, due to the boundary conditions at r_1 and r_{n+1}.

$$\frac{dT_{mid1}}{dt}=\frac{-Q_{cond2}+Q_{joule1}-Q_{rad1}}{C_{therm1}} \quad (22)$$

$$\frac{dT_{midj}}{dt}=\frac{Q_{condj}-Q_{cond(j+1)}+Q_{joulej}-Q_{radj}}{C_{thermj}},2\le j\le n-1 \quad (23)$$

$$\frac{dT_{midn}}{dt}=\frac{Q_{condn}-Q_{cond(n+1)}+Q_{joulen}-Q_{radn}}{C_{thermn}} \quad (24)$$

Equations (25) to (28) define the terms used in the differential equations.

$$C_{thermj}=A_jC_p(T_{midj})\rho(T_{midj}) \quad (25)$$

$$Q_{cond(n+1)} = \frac{T_{water} - T_{midn}}{R_{out(n+1)}} \quad (26)$$

$$Q_{joulej} = A_j E(t)^2 \sigma(T_{midj}) \quad (27)$$

$$Q_{radj} = A_j 4\pi\varepsilon_0(T_{midj}) \quad (28)$$

The outer boundary condition is the water wall temperature. The inner boundary condition cannot be chosen to be at r=0 since equation () becomes singular. However, at a distance δ from the centre it is reasonable to assume that the heat flux and radiation flux is vanishingly small.

It remains to model equation (12) for the electrical field. In terms of the shells, it is $i_{in}(t) = E(t)G_{arc}(t)$ where

$$G_{arc} = \sum_{j=1}^{n} A_j \sigma(T_{midj}) \quad (29)$$

Using (29) would result in a differential algebraic system with n ODEs and one algebraic equation. Differential algebraic systems cannot be solved via standard approaches such as MATLAB's Simulink, and for this reason, it is advantageous to include a parasitic electrical capacitance C_{in} in parallel with the electrical circuit.

$$\frac{\partial E}{\partial t} = \frac{i_{in} - EG_{arc}}{C_{in}} \quad (30)$$

This parasitic capacitance would exist in a real lamp, although it would be so small that it would have a negligible effect on the circuit behavior. Including a parasitic capacitance creates a system of $n+1$ differential equations for which a wider variety of numerical solvers can be used. This is in line with the goal of defining a model that can be used in a practical circuit design.

The outputs of the model are the total arc conductance (29) and the total radiation up to an (arbitrary) time t:

$$Q_{rad\_arc}(t) = \int_0^t \sum_{j=1}^{n} Q_{radj}(s)ds \quad (31)$$

III. Circuit Implementation

It would be advantageous to be able to import the arc model into a circuit simulator in order to more easily design and test a power source for the arc. A Simulink circuit implementation of the ordinary differential model was therefore designed and simulated. The construction of the needed temperature-dependent resistors and capacitors is now presented.

A. Material Properties

Five temperature-dependent material properties, $\sigma(T)$, $\kappa(T)$, $C_p(T)$, $\rho(T)$, and $\varepsilon_0(T)$ appear in the energy balance equation (1) and (2). Because $C_p(T)$ and $\rho(T)$ never appear separately in the equations used, but only as a product, the function $C_p(T)\,\rho(T)$ is treated as a single function. In all of the models simulated, known material properties of argon gas at 8 bar are used for these functions. This pressure corresponds approximately to the environment expected for the vortex water-wall arc lamp. The functions were available in tabular form at 100K intervals and were implemented using linearly-interpolated lookup tables [7].

B. Circuit Model of Temperature-Dependent Thermal Resistors

The series thermal resistors were implemented using a dependent current source. R_{outj} and $R_{in(j+1)}$ are directly connected in series, and so are implemented using one current source (Figure 5). The circuit shown in Figure 4 implements equation (32)

$$i = v\left(\frac{1}{G_1(v_1)} + \frac{1}{G_2(v_2)}\right)^{-1} \quad (32)$$

C. Circuit Model of Temperature-Dependent Capacitor

Implementing a non-linear capacitor adds extra complexity as there must be a differential or integral component in the model. Integral components are advantageous as they are more stable, so in the case of a capacitor the current-dependent voltage source implementation is preferred. However, this means that the capacitor must be modeled using a charge-based model.

By definition the relationship between the voltage across a capacitor and the current through it is given by (33a).

$$i(t) = \frac{d\Phi}{dt} = \frac{dh(v)}{dv}\frac{dv}{dt} = C(v)\frac{dv}{dt} \quad (33a)$$

Charge Φ is a function of voltage $\Phi = h(v)$, so

$$i(t) = \frac{d\Phi}{dt} = \frac{dh(v)}{dv}\frac{dv}{dt} = C(v)\frac{dv}{dt} \quad (33b)$$

If the equation is integrated then:

$$\int_0^t i(s)ds = \int_0^t \frac{dh(v)}{dv}\frac{dv(s)}{dt}ds = h(v(t)) - h(v(0)) \quad (34)$$

$$\Phi(t) = h(v(t)) = \int_0^t i(s)ds + h(v(0)) \quad (35)$$

If the charge Φ is an increasing function of the voltage v then the voltage is a function of the charge: $v = g(\Phi)$ for some g. That is,

$$v(t) = g\left(\int_0^t i(s)ds + h(v(0))\right) \quad (36)$$

(In the special case of a voltage-independent capacitor $C(v) = C_0$, then $h(v) = C_0 v$ and $g(\Phi) = \Phi/C_0$.) A Simulink implementation of the charge-based capacitor (36) is shown in Figure 6. For this model, h = Cρ. It and its inverse are found by linear interpolation from the data obtained from [7].

The remaining resistors and current sources are implemented similarly using dependent current sources and appropriate linearly extrapolated lookup tables.

IV. Simulations

A. Approach Used for Validation of Model

The energy balance equation (11-12) for an arc lamp is well known from the literature [8] and is assumed to be valid. In this section, the finite volume method (FVM) model

(equations (22-24), (30)) is tested against the finite element method (FEM) model of equations (11-12). All FEM modeling was done in COMSOL Multiphysics, while FVM modeling was done using MATLAB's ode15s ODE solver or (when stated) in MATLAB's Simulink. Rather than computing the 3-d equation (11), the 1-d reduction to radial coordinates is computed. The FEM model is always computed with a large number of elements, resulting in a highly accurate numerical solution to the energy balance equation (11-12). For all FEM and FVM modeling, the material constants $C_p(T)$, $\rho(T)$, $\kappa(T)$, $\varepsilon_0(T)$, and $\sigma(T)$ were found via linear interpolation based on known properties of argon gas at a pressure of 8 bar [7]. In all simulations, the temperature at the outer wall is 300K, the radius of the arc, R, is 45mm, and the inner-most radius, δ, is 0.1mm.

Several steady state simulations of the FEM model were also initially compared to expected results for a radiation-dominated lamp as a means of validating the FEM model.

B. Finite Element Method Model

Steady state and transient FEM simulations were run in order to establish the behavior of the arc under different conditions. Figure 7 shows the temperature profile for a radial cross-section of the arc in response to a sinusoidal input pulse. Before the pulse, the lamp was in the steady state corresponding to a constant simmer current of 400A. The input pulse was superimposed on this current.

In this case, although the arc retains an isothermal core which rises and falls in temperature, the heat capacity of the arc prevents the pulse from affecting the outer edges of the arc. As shown in Figure 7, the core width expands at a much slower rate than the rate with which the core temperature rises and falls; in this case, the core never fully fills the lamp. The lamp cools much more slowly than it heats, and continues to radiate for some time after the end of the current pulse.

C. Finite Volume Method Model

Steady-state and transient simulations were run based on the FVM model described in equations (22-24), (30).

First, it was checked that the FVM model converges to a continuous solution as the number of regions becomes large. The steady state for the 400A simmer current was computed using an increasing number of regions. The temperature at a given point in space can be calculated and the results compared for different numbers of regions to track the behavior at a single point as n becomes large. Division of the arc into 12, 36, 108, and 324 regions was used to track the behavior of 12 points equidistant along the radius as n increased. The error was found to decrease at a rate of $1/n^{1.6}$. A justification for the formula used in equation (37) may be found in ([6], p.292).

$$\frac{T(r)_{36}-T(r)_{12}}{T(r)_{108}-T(r)_{36}} \approx \frac{T(r)_{108}-T(r)_{36}}{T(r)_{324}-T(r)_{108}} \approx 6 \approx 3^{1.6} \qquad (37)$$

Next, a tanh function

$$i_{in}(t) = 400 + 29800(1+\tanh(2\pi(t-.05)))$$

was used as an input current to investigate the transient model behavior with differently sloped time-varying input currents and a different number of elements. Element temperatures and arc voltage are shown for an increasing number of elements in Figures 8 and 9.

At certain points in time, there is a sudden small drop in the temperature and voltage in all regions. When the current through the arc is raised, the inner regions of the arc rise in temperature, and the isothermal core widens. As it widens, adjoining regions become hotter and join the isothermal core. As the core expands nearer to the outer radius of the lamp, this transition becomes increasingly abrupt. When an outer element's temperature undergoes a large increase very quickly, the core temperature drops very slightly.

These drops in temperature and voltage remain the same size regardless of the error tolerances set in ode15s. And so, they appear to be an artifact of the finite volume method. When compared with FEM simulations using the same number of elements, the same error tolerances, and linear fitting functions, the finite volume method results for the temperature at r = 0 slightly overshoot the more accurate FEM result and then drops down slightly below the FEM result (Figure 9). As the number of regions is increased, the FVM steps become smoother and the two models become increasingly similar.

Small sudden changes in the solution are seen when there is a large and abrupt temperature change in a region. It may be feasible to remove this high frequency behavior without significantly changing the arc behavior on the time scale of interest, for example with the introduction of small parasitic elements linking each region in a form of feed forward filtering. This possibility should be explored.

D. Finite Volume Method with LC Pulse-forming Network

The FVM model is now expanded to include a simple LC pulser circuit, as shown in Figure 10. I_{ss} represents the simmer current which remains between pulses and maintains the arc. The capacitor C_{ch} is initially charged with a voltage V_{ch}. The switch is closed to begin the pulse, and is reopened at the next zero-crossing of the pulser current i_L. The resulting current pulse through the arc model is a nearly sinusoidal pulse and is a half a period in duration.

The differential equations describing the circuit are (22)-(24) and (38) for the arc itself, with i_{in} in equation (30) replaced by $I_{ss} + i_L(t)$, giving

$$\frac{dE}{dt} = \frac{i_L + I_{ss} - EG_{arc}}{C_{in}} \qquad (38)$$

and equation (39) and (40) for the pulser, shown to the left of the arc in Figure 11. The variable '*switch*' is set to 1 to close the switch, and reset to 0 at the next zero-crossing of the inductor current i_L to reopen the switch. The initial data is $v_{ch}(0)=V_{ch}$ and $i_L(0)=0$. This results in a single pulse.

$$\frac{dv_{ch}}{dt} = \frac{-i_L}{C_{ch}} \bullet switch \qquad (39)$$

$$\frac{di_L}{dt} = \frac{v_{ch} - E}{L_{ch}} \bullet switch \tag{40}$$

It remains to find reasonable values for L_{ch}, C_{ch}, and V_{ch}. This is done by considering the LC circuit in isolation from the arc lamp. It has a pulse width

$$PW = \pi\sqrt{L_{ch}C_{ch}} \tag{41}$$

The total energy stored in the electric field of the capacitor is transferred to the magnetic field of the inductor, which provides the pulse current for the arc. For an initial approximation, the loss caused by the arc resistance may be ignored. The pulser voltage and current, $v_{ch}(t)$ and $i_L(t)$ are assumed to be approximately sinusoidal with peak amplitudes of V_{ch} and I_L respectively. Thus the total energy is (42):

$$E_J = \frac{C_{ch}V_{ch}^{\ 2}}{2} = \frac{L_{ch}I_L^2}{2} \tag{42}$$

Given a desired pulse width, PW, and peak current, I_L, one can find L_{ch}, C_{ch}, and V_{ch} that satisify equations (41) and (42), leaving one degree of freedom.

E. Simulation Results

Simulation results for a circuit with L_{ch} = 160µH and C_{ch} = 500µF, with charging voltage V_{ch}=15kV, were compared to a well-resolved solution of the FEM model. Since a charging circuit cannot easily be added to the FEM model, the FEM model was run using a sinusoidal input current with amplitude and period chosen to match the current observed in the ODE model with the pulser.

The temperature at the centre of the arc, T_{mid1}, is plotted in Figure 12, and the electric field in Figure 13. Two versions of the FVM model were ultimately simulated: one solved the differential equations directly in MATLAB, and the second was a Simulink circuit implementation. Figure 14 compares the arc radiation output for the two different FVM implementations and the FEM model.

The radiation dose at some particular time is the most important final metric, as it dictates the amount of heat transferred to the wafer. This is $Q_{rad\_arc}(s)$ (31) integrated from time 0 to time T. The radiation dose at several points in time is tabulated in Table 1 with the different models. Although more elements give higher accuracy, at 12 elements the worst error in dosage is less than 0.4% for this pulse. The FEM model is taken as the exact solution in defining this error.

The simulations were done with regions spaced at increments of equal radius. As seen in Figure 7, for pulsed operation superimposed on an initial simmer current, a large central portion of the arc rises and falls essentially as one, without significant radial temperature gradients.

V. Conclusions

A finite volume arc model was derived using averaging of the energy balance equation over spatial domains. The space averaging approach accurately models the PDE form of the energy balance equation, with both steady state and transient arc currents, including high energy pulses with a current amplitude range from 400A to 40kA and a pulse width of a millisecond or less.

The developed spatially averaged model uses physical and geometric data to set the coefficients in the equations thus avoiding the problem of system identification. This model is in a form that can be expressed in circuit form, while giving the expected temporal v versus i and optical output characteristics.

Optimization of the spacing of regions would be expected to result in greater accuracy with a smaller number of regions. A smaller number of regions could be used near the centre of the lamp, with more densely spaced regions near the outer radius where there is a strong radial dependence of temperature.

References

[1] T. Thrum, D. Camm, S. Dets, A.Hewett, I. Rudic, G.C. Stuart, A. Viel, "Development of a powerful vortex stabilized waterwall flash lamp for RTP applications," Industry Applications Conference, Conference Record of the 39th IAS Annual Meeting, vol 2, no 3-7, Oct. 2004 pp. 1019 – 1023

[2] "High Performance Flash and Arc Lamps" PerkinElmer Optoelectronics www.perkinelmer.com/opto.

[3] Ruben D. Garzon, "High Voltage Circuit Breakers: Design and Applications" 2nd ed., New York: Marcel Dekker, Inc., 2002.

[4] Niklas Gustavsson, "Evaluation and Simulation of Black-box Arc Models for High Voltage Circuit-breakers', unpublished Master's Thesis, Department of Electrical Engineering, Linkoping: Linkoping University, 2004.

[5] Kendall E. Atkinson, "An Introduction to Numerical Analysis," 2nd ed., New York: Wiley, 1989.

[6] F.P. Incropera, D.P. DeWitt, T.L. Bergman, A.S. Lavine, "Introduction to Heat Transfer," 5th ed., New York: Wiley, 2007.

[7] "Material Property Database", Jahm Software, http://www.jahm.com.

[8] J. J. Lowke, "Characteristics of Radiation-Dominated Electric Arcs," Journal of Applied Physics, vol 41, no. 6, May 1970, pp. 2588-2600.

TABLE 1 - TOTAL RADIATION DOSE FROM ONSET OF SIMULATION TO GIVEN TIME

Integral of Qrad (kJ)	MATLAB 12 elements	Simulink 12 elements	MATLAB 24 elements	COMSOL 240 elements	COMSOL 480 elements
at 1ms	15.06	15.09	15.02	15.03	15.04
at 2ms	17.02	17.06	17.00	17.04	17.05
at 3ms	17.51	17.53	17.44	17.50	17.50

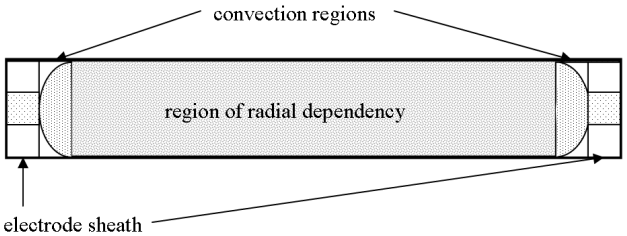

Figure 1 - View of lamp showing end effects and conduction regions

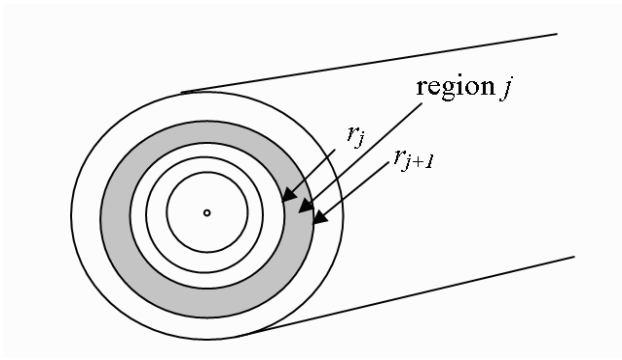

Figure 2 - Problem domain and regions. The shaded region between $r = r_j$ and $r = r_{j+1}$ is region 'j'

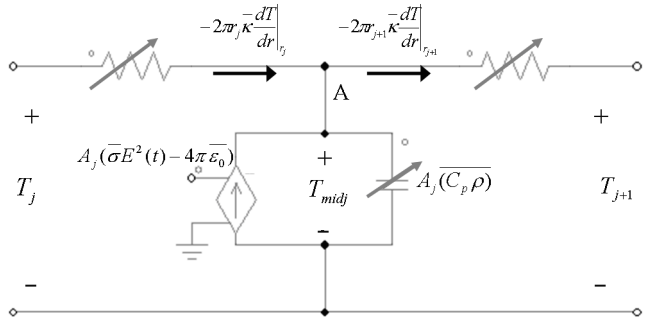

Figure 3 - Thermal circuit representation of one ring-shaped arc region

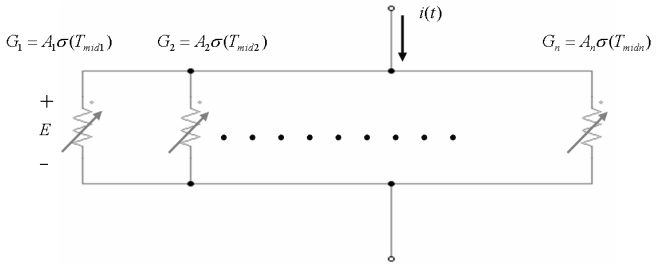

Figure 4 – Electrical circuit for n-region arc model

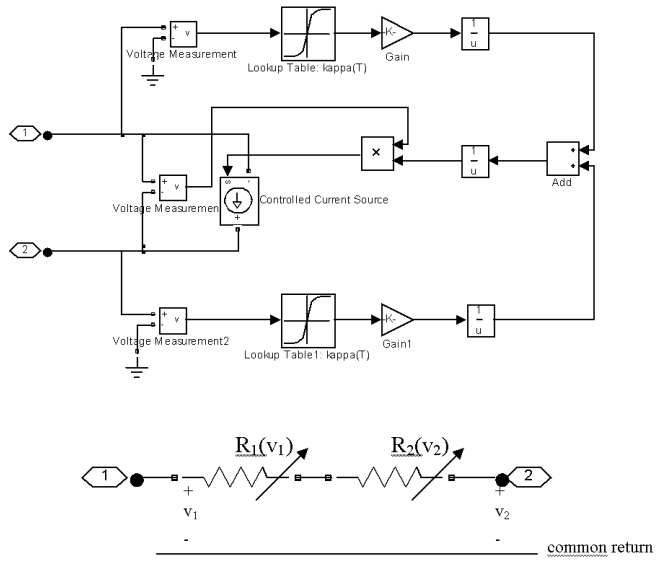

Figure 5 – (top) Simulink implementation of two voltage dependent resistors in series, and (bottom) equivalent circuit.

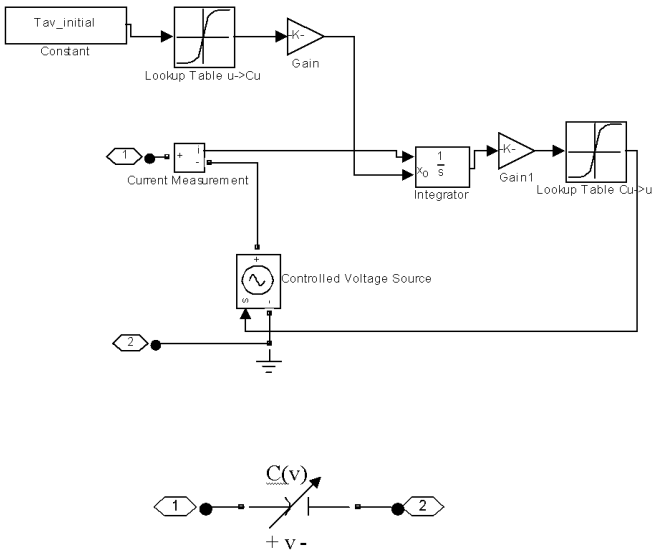

Figure 6 – (top) Simulink implementation of voltage dependent capacitor, and (bottom) equivalent circuit.

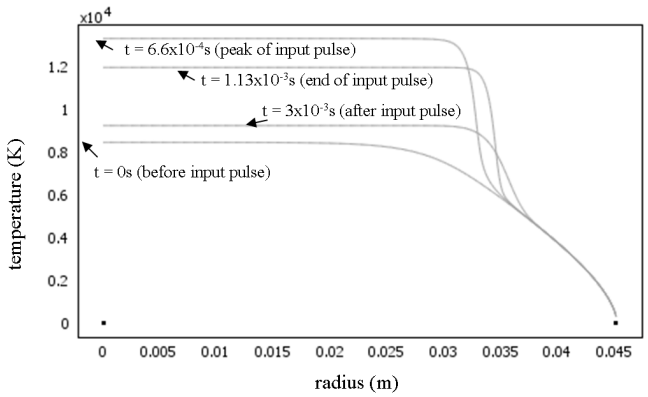

Figure 7 –Temperature as a function of arc radius for different points in time in response to a current pulse. A sinusoidal pulse with a peak current of 40kA and a 1.125ms pulse width is superimposed on a constant baseline current of 400A.

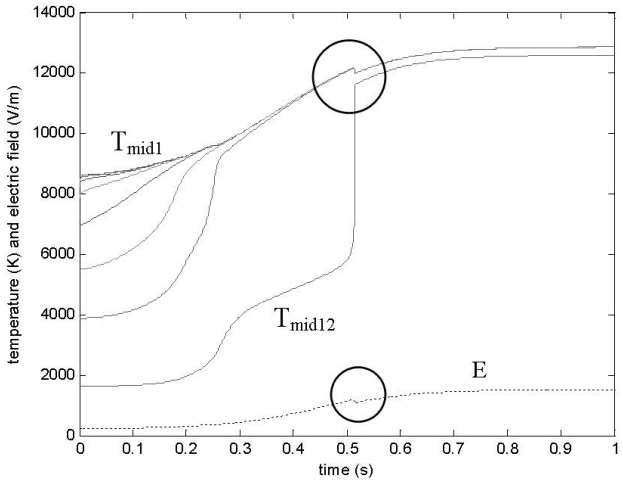

Figure 8- Temperature for each region and arc electric field for a tanh current where n=12. A sudden drop in values may be seen in the circled areas.

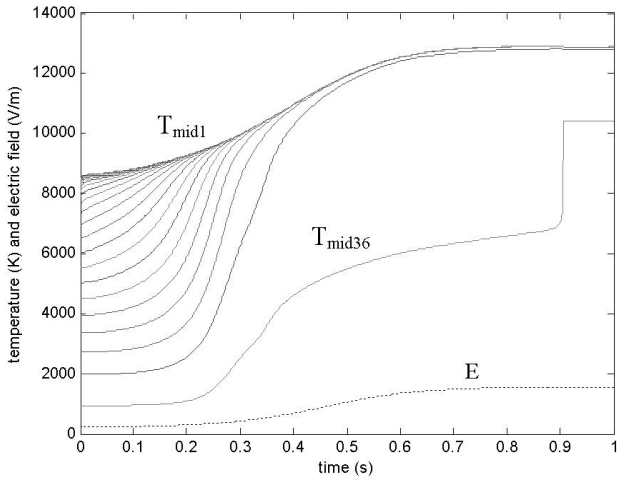

Figure 9 - Temperature for each region and arc electric field for a tanh current where n=36.

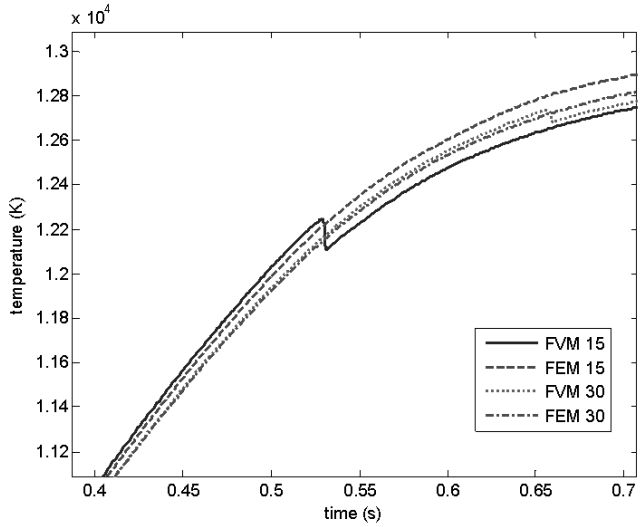

Figure 10 – Comparison of FVM and FEM temperature responses as a function of time for the innermost region (T_{midl}).

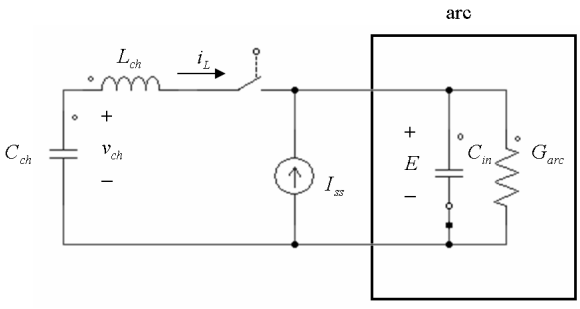

Figure 11 – Arc model including pulse forming circuit

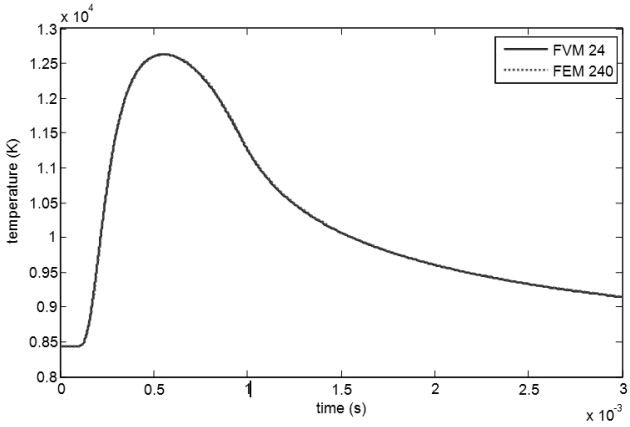

Figure 12 - Central temperature in response to a 56.25kJ pulse. FEM with 240 elements is overlaid on the same graph as FVM (equation based model) with 24 elements.

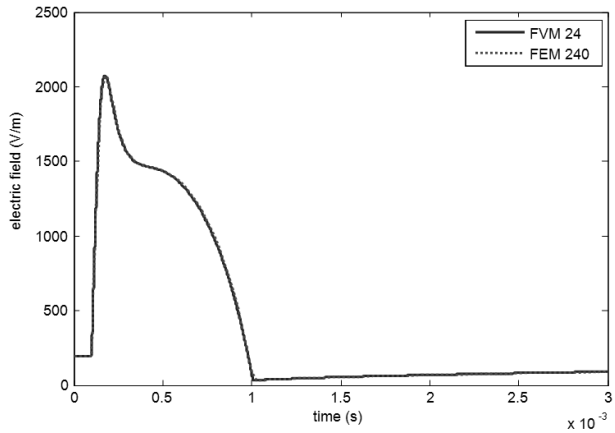

Figure 13 - Arc electric field in response to a 56.25kJ pulse. FEM with 240 elements is overlaid on the same graph as FVM (equation based model) with 24 elements.

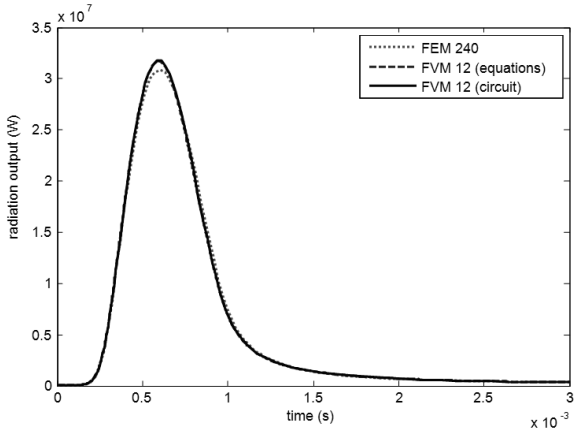

Figure 14 – Arc radiation in response to a 56.25kJ pulse. Comparison of 12 element FVM with 240 element FEM. The 12 element FVM has a slightly higher peak radiation.